Measurement and Control of Single Nitrogen-Vacancy Center Spins above 600 K

D. M. Toyli,[1] D. J. Christle,[1] A. Alkauskas,[1,2] B. B. Buckley,[1] C. G. Van de Walle,[1,2] and D. D. Awschalom[1,*]

[1]*Center for Spintronics and Quantum Computation, University of California, Santa Barbara, California 93106-6105, USA*

[2]*Materials Department, University of California, Santa Barbara, California 93106-5050, USA*

(Received 13 January 2012; published 5 July 2012)

We study the spin and orbital dynamics of single nitrogen-vacancy (NV) centers in diamond between room temperature and 700 K. We find that the ability to optically address and coherently control single spins above room temperature is limited by nonradiative processes that quench the NV center's fluorescence-based spin readout between 550 and 700 K. Combined with electronic structure calculations, our measurements indicate that the energy difference between the ^3E and $^1A_1$ electronic states is approximately 0.8 eV. We also demonstrate that the inhomogeneous spin lifetime (T_2^*) is temperature independent up to at least 625 K, suggesting that single NV centers could be applied as nanoscale thermometers over a broad temperature range.

DOI: 10.1103/PhysRevX.2.031001 Subject Areas: Quantum Information, Semiconductor Physics, Spintronics

The negatively charged nitrogen-vacancy (NV) center spin in diamond stands out among individually addressable qubit systems because it can be initialized, coherently controlled, and read out at room temperature [1]. The defect's robust spin coherence [2] and optical addressability via spin-dependent orbital transitions [3] have enabled applications ranging from quantum information processing [4–7] to nanoscale-magnetic and electric-field sensing [8–10]. While it has been shown that NV center spins can be optically polarized up to at least 500 K [11,12], little is known about what processes limit the spin's optical addressability and coherence at higher temperatures. Understanding these processes is important to high-temperature field-sensing applications and will aid the search for new defect-based spin qubits analogous to the NV center [13,14] by identifying the aspects of its orbital structure responsible for its high-temperature operation.

The NV center's optical-spin polarization and optical-spin readout result from a spin-selective intersystem crossing (ISC). Although optical transitions between the spin-triplet ground ($^3A_2$) and excited (^3E) states [1.945 eV zero-phonon line (ZPL)] are typically spin conserving, the ^3E state can also relax to the $^3A_2$ state via an indirect pathway that involves a nonradiative, triplet to singlet ISC and subsequent transitions through at least one additional singlet [Fig. 1(a)]. The ^3E ISC is much stronger for the $m_s = \pm 1$ ^3E sublevels than for the $m_s = 0$ sublevel, which facilitates spin readout through the resulting spin-dependent photoluminescence (PL) and initializes the spin into the $m_s = 0$ $^3A_2$ sublevel with high probability ($P_{m_s=0} \sim 0.8$) through repeated optical excitation [15]. Despite the singlet pathway's critical role in preparing and interrogating the spin, open questions remain regarding the number and energies of the singlets involved. Recent experiments have established that it consists of at least two singlets of $^1A_1$ and ^1E symmetry separated by 1.19 eV [16–18], and have shown that the ^1E state lifetime is strongly temperature dependent below 300 K [17,19]. The details of the ^3E ISC remain uncertain, however, given computations that suggest the singlet pathway involves three singlets [20] and the lack of direct measurements of the ^3E to singlet transition energy.

In this work, we report measurements of single NV center spins between 300 and 700 K. We show that thermally activated nonradiative processes diminish the spin selectivity of the ^3E ISC and quench the optical-spin readout above 550 K. Our measurements indicate the energy barrier for nonradiative relaxation from the ^3E state is approximately 0.5 eV. We perform electronic structure calculations that suggest an orbital structure consistent with a two-singlet decay pathway, the measured energy barrier for nonradiative relaxation, and the temperature dependence of the ^1E state lifetime. Furthermore, we demonstrate that the spin coherence remains robust even as nonradiative processes quench the optical-spin readout. In addition to demonstrating the defect's potential for high-temperature magnetic-field-sensing applications, these results suggest single NV centers could act as nanoscale thermometers with sensitivities on the order of 100 mK/$\sqrt{\text{Hz}}$ between room temperature and 600 K. This high sensitivity and wide range of operating temperatures make NV centers an attractive candidate for a variety of thermosensing applications such as cellular thermometry [21] and diamond-based scanning thermal microscopy [22].

To study single NV centers at elevated temperatures, we constructed devices that combine on-chip heating and thermometry elements, solid immersion lenses (SILs) for

*Corresponding author
awsch@physics.ucsb.edu

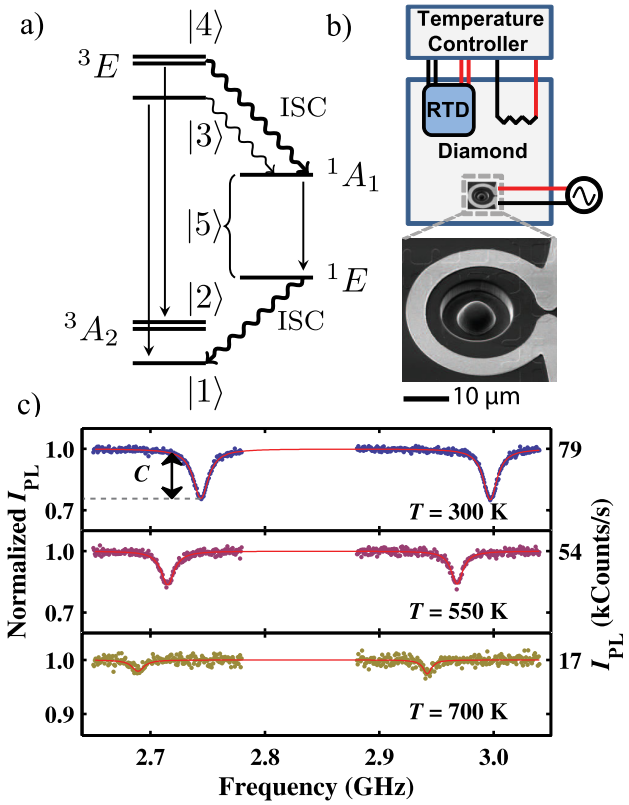

FIG. 1. (a) Orbital diagram showing the triplet ($^3A_2$ and ^3E) and singlet ($^1A_1$ and ^1E) electronic states. The straight lines represent optical transitions and the snaked lines represent nonradiative intersystem crossings (ISC). Bra-ket notation denotes the effective levels used to model the photoluminescence intensity (I_{PL}) and electron spin resonance (ESR) contrast. Level $|2\rangle$ ($|4\rangle$) is a grouping of the $^3A_2$ (^3E) $m_s = \pm 1$ sublevels and $|5\rangle$ is an effective singlet level. (b) Sample schematic showing the resistive heater and resistive temperature detector (RTD), the solid immersion lens (SIL), and the antenna. The scanning electron microscope image shows the SIL and antenna. (c) I_{PL} of a single NV center versus applied microwave frequency. Lorentzian dips with normalized amplitude C are observed at the spin resonance frequencies ($B \sim 45$ G). The left (right) axis shows the normalized (absolute) I_{PL} to illustrate the temperature-dependent decrease in C and I_{PL}. The red lines are two-Lorentzian fits. The crystal field splitting (D) is the average of the resonance frequencies. The measurements were performed at high microwave power to saturate the spin transitions.

enhanced photon collection efficiency [23,24], and on-chip microwave elements for spin control [Fig. 1(b)] [25,26]. We studied NV centers in a single-crystal diamond sample ($[N]_S^0 < 5$ ppb) using a home-built confocal microscope [27]. We etched hemispherical SILs around single defects with a focused ion beam, patterned microwave antennas around the NV centers, and patterned a resistive heater on the sample surface. We adhered a commercial resistive temperature detector (RTD) to the diamond and connected the heater and RTD to a temperature controller to achieve stability within ± 50 mK up to 700 K in air.

Continuous-wave (CW) electron spin resonance (ESR) measurements revealed that the NV center's PL intensity (I_{PL}) and relative I_{PL} difference between its spin states (ESR contrast) strongly decrease above 550 K. The measurements were carried out by applying a swept-frequency ac magnetic field while monitoring I_{PL} under continuous 532-nm laser excitation. We observed Lorentzian dips in I_{PL} with normalized amplitude C centered at the ground-state spin resonance frequencies [3]. The resonance frequencies are determined by the crystal field splitting (D) between the $m_s = \pm 1$ and $m_s = 0$ states, and the Zeeman shift due to an applied magnetic field [28]. We applied an approximately 45 G magnetic field along the defect's symmetry axis to separate the $m_s = \pm 1$ states by approximately 250 MHz. We observed shifts in D on the order of 100 kHz/K due to lattice expansion, which is consistent with measurements performed at lower temperatures [29,30]. In addition to this shift, both C and the off-resonant I_{PL} showed a pronounced decay above 550 K; by 700 K the Lorentzian dips were barely observable and the off-resonant I_{PL} dropped to approximately 20% of its room-temperature value [Fig. 1(c)].

Thermal quenching of a point defect's I_{PL} often results from thermally activated nonradiative processes that shorten the effective optical lifetime of an emitter [31]. Previous ensemble measurements of the temperature dependence of the NV center's optical lifetime in bulk diamond [32] and nanodiamonds [33] have shown conflicting results. We therefore measured the spin-resolved excited-state lifetimes ($\tau_{m_s=0}$ and $\tau_{m_s=\pm 1}$) for a single NV center as a function of temperature following the method of Ref. [19] to investigate their influence on ESR contrast and I_{PL} [Fig. 2]. The spin dependence of the ^3E ISC preferentially shortens $\tau_{m_s=\pm 1}$ and thus optical excitation leads to biexponential fluorescence decay, where the decay constants correspond to $\tau_{m_s=0}$ and $\tau_{m_s=\pm 1}$ and the relative amplitudes reflect the spin polarization. To probe the lifetimes, we initialized the spin into $m_s = 0$ using a 1.4 μs

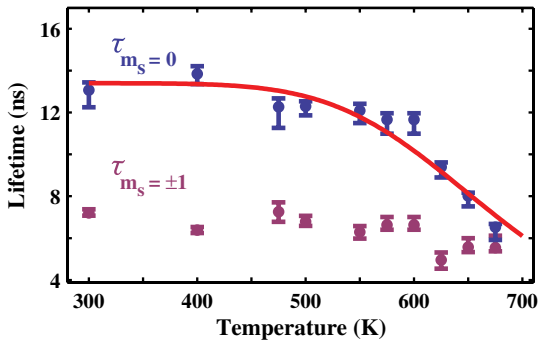

FIG. 2. Temperature-dependent excited-state lifetimes, $\tau_{m_s=0}(T)$ (blue) and $\tau_{m_s=\pm 1}(T)$ (magenta), for a single NV center. The error bars reflect fitting uncertainties (68% intervals). The red line is the Mott-Seitz formula for $\tau_{m_s=0}(T)$ with $\tau_{m_s=0}(300\text{ K}) = 13.4$ ns, $s_{m_s=0} = 3420$, and $\Delta E = 0.48$ eV.

pulse from a 532-nm laser. After waiting 500 ns for the singlets to depopulate, we applied a resonant microwave pulse to rotate the spin into a superposition of $m_s = 0$ and $m_s = -1$. We then applied a 555-nm picosecond laser pulse and measured the resulting PL with a time-correlated photon counting module. We repeated this measurement for varying spin rotation angles and performed global Bayesian inference to infer $\tau_{m_s=0}$, $\tau_{m_s=\pm1}$, and the finite spin polarization at each rotation angle from the measurements (see Supplemental Material [26] and Refs.). Above 550 K, $\tau_{m_s=0}(T)$ showed a sharp reduction with increasing temperature. In spite of this, we found that the ground-state spin polarization after optical pumping was temperature independent within our measurement uncertainty up to 650 K [26].

We find that $\tau_{m_s=0}(T)$ is accurately described by the Mott-Seitz formula for nonradiative relaxation via multiphonon emission [31],

$$\tau_{m_s=0}(T) = \frac{\tau_{m_s=0}(300\ \mathrm{K})}{1 + s_{m_s=0}\exp\left[-\frac{\Delta E}{k_B T}\right]}, \qquad (1)$$

where $1/\tau_{m_s=0}(300\ \mathrm{K}) = 1/\tau_{\mathrm{rad}} + k_{m_s=0}$. Here $1/\tau_{\mathrm{rad}}$ is the radiative rate, $k_{m_s=0}$ is the room-temperature nonradiative transition rate from the ^3E $m_s = 0$ sublevel to the uppermost singlet state [Fig. 1(a)], $s_{m_s=0}$ is the frequency factor, and ΔE is the energy barrier for the nonradiative process. From a fit to $\tau_{m_s=0}(T)$, we find $\tau_{m_s=0}(300\ \mathrm{K}) = (13.4 \pm 0.6)$ ns, $s_{m_s=0} < 1.64 \times 10^4$, and $\Delta E = (0.48^{+0.15}_{-0.13})$ eV. In general, ΔE is interpreted via a one-dimensional configuration coordinate diagram. These diagrams show the dependence of total energies in different electronic states as a function of a generalized configuration coordinate ΔR. The latter measures the total displacement of all atoms along the path that interpolates between equilibrium geometries in the relevant electronic states. ΔE is then classically defined as the energy difference between the intersection point of two potential energy curves and the energy minimum of the upper curve. In such a scenario, nonradiative relaxation is interpreted as a phonon-assisted process over the energy barrier.

We combine our measurement of ΔE with electronic structure calculations to construct a configuration coordinate diagram for the NV^- center in its $^3A_2$, ^3E, $^1A_1$, and ^1E electronic states. The theoretical methodology employed relies on the use of supercells to describe defects and hybrid density functionals for an accurate treatment of the electronic structure [13,39]. Additional details regarding the computational methods are provided in Supplemental Material [26] and Refs. [40–47]. The calculated ZPL between the triplet states, 1.972 eV, agrees favorably with the experimental value of 1.945 eV. In Fig. 3, we placed the minima of $^3A_2$ and ^3E states according to the experimental ZPL with zero defined by the $^3A_2$ state's equilibrium energy. We mapped the potential energy surfaces for these

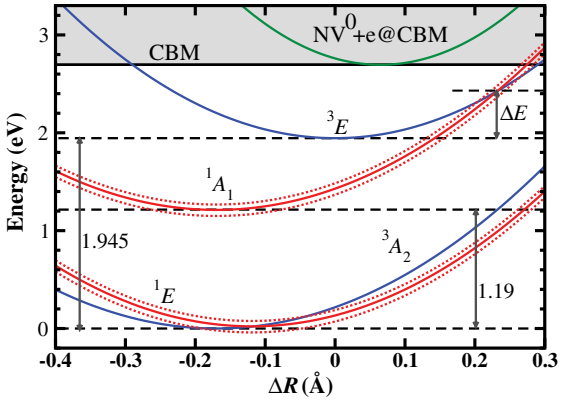

FIG. 3. Configuration coordinate diagram of the NV^- center. ΔR measures the total displacement of all atoms along the path that interpolates between equilibrium geometries in the $^3A_2$ and ^3E electronic states. All energies are relative to the $^3A_2$ state's equilibrium energy. We placed the $^1A_1$ state based on the assumption that its equilibrium atomic configuration and vibrational frequencies were similar to those of the $^3A_2$ state and using our measurement of ΔE. The ^1E state was placed 1.19 eV below the $^1A_1$ state based on their known energy difference. The uncertainties in the $^1A_1$ and ^1E energies reflect the uncertainty in ΔE (68% interval, dotted red lines). The triplet (1.945 eV) and singlet (1.19 eV) zero-phonon lines are also indicated.

two states along the path that linearly interpolates between their equilibrium geometries. The resulting Stokes and anti-Stokes shifts were 0.27 and 0.23 eV, respectively.

In constructing the configuration coordinate diagram for the singlet states, we also assumed that the $^1A_1$ state's equilibrium atomic configuration and vibrational frequencies were equal to those of the $^3A_2$ state. Indeed, the $^1A_1$ state's $a_1^2e^2$ electron configuration [48,49] implies the two states have a similar electron density. In turn, this implies that the ionic forces are similar for these two states away from their equilibrium geometries. Therefore, we conclude that the Huang-Rhys factor (S), the average number of nonequilibrium phonons emitted when the electronic state changes [31], for the ^3E to $^1A_1$ transition, is the same as that for the ^3E to $^3A_2$ optical transition. For the latter, our calculations give a value of $S \approx 3.2$, close to the value of $S \approx 3.65$, which is inferred from the relative spectral weight of the ZPL with respect to the phonon sideband [50]. The value $S > 1$ for the ^3E to $^1A_1$ transition confirms our hypothesis, implied in Eq. (1), that the ISC is accompanied by multiphonon emission.

We interpret ΔE as the energy difference between the intersection point of the ^3E and $^1A_1$ potential energy curves and the energy minimum of the ^3E state. This places the $^1A_1$ state (0.76 ± 0.07) eV below the ^3E state. By fixing ΔE based on our measurements, our analysis avoids difficulties in computing the absolute energies of the singlet states resulting from their multideterminant electronic wave functions [48,49]. We place the ^1E state 1.19 eV below the $^1A_1$ state [16–18] and find that the ^1E singlet is

close in energy to the $^3A_2$ triplet. Since the $^3A_2$ state is the ground state, the ^1E state should be higher in energy. Within the uncertainty in ΔE, the configuration coordinate diagram fulfills this constraint and indicates that only small energy barriers for nonradiative relaxation from the ^1E state are possible in qualitative agreement with energy barriers inferred from the temperature dependence of the ^1E state lifetime [17,19].

To demonstrate that the neutral charge state of the NV center (NV^0) does not interfere in the temperature-activated nonradiative processes discussed above, in Fig. 3 we also placed the potential energy curve for the NV^0 center in its ^2E ground state based on the charge-state transition levels given in Ref. [13] and the calculated total-quadratic distortion ΔR. The resulting high ionization potential for the NV^- center in the ^3E state (> 0.8 eV) shows that the escape of the electron to the conduction band minimum is negligible for the temperatures studied.

Our inference of the $^1A_1$ and ^1E energies is influenced by our classical interpretation of ΔE, which is based on the consideration of a single effective phonon mode of a_1 symmetry that strongly couples to the distortion of the defect [31]. In fact, the temperature-activated ISC from the ^3E $m_s = 0$ state to the $^1A_1$ state also requires coupling to phonons of e symmetry, which is unnecessary for the ISC from the ^3E $m_s = \pm 1$ states [18]. Nevertheless, the presented model is a good approximation that provides a suitable description of the temperature-dependent ISC. The generalization of this model, which takes into account quantum effects as well as coupling to phonons of different symmetry during radiative and nonradiative processes, will be presented elsewhere [51].

Having interpreted ΔE, we employ a model of the ESR experiments using the density matrix formalism that includes dissipation to reveal that the observed decreases in C and I_{PL} are predominantly caused by the temperature dependence of $\tau_{m_s=0}$ and $\tau_{m_s=\pm 1}$ [52]. The model consists of irreversible transitions between five effective energy levels [Fig. 1(a)] under optical pumping with an off-diagonal term to capture the coherent microwave driving [26]. The only temperature-dependent components are $\tau_{m_s=0}$, $\tau_{m_s=\pm 1}$, and the known temperature dependence of the effective singlet lifetime [19]. The model shows agreement with our measurements of $C(T)/C(300\ \mathrm{K})$ and $I_{PL}(T)/I_{PL}(300\ \mathrm{K})$ [Fig. 4]. It reveals that the small decrease in C below 550 K is due to the shortening of the singlet lifetime, while the decreases in both C and I_{PL} above 550 K are primarily caused by the thermally activated nonradiative processes that shorten $\tau_{m_s=0}$ and $\tau_{m_s=\pm 1}$.

We established from pulsed ESR measurements that the NV center remains spin coherent even as nonradiative processes diminish the ESR contrast and I_{PL}. The spin's robust coherence is due to the equal population of the sublevels of the ^{13}C nuclear spin impurities which

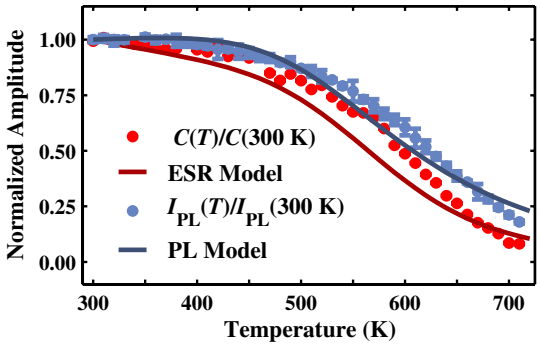

FIG. 4. Temperature-dependent ESR contrast [$C(T)$, red points] and $I_{PL}(T)$ (blue points). Both quantities were normalized by their 300 K values (~ 0.22 and ~ 80 kCps, respectively). $C(T)$ was determined from fitting the CW ESR data and I_{PL} was determined from Gaussian fits to confocal microscopy line scans. The solid lines represent predictions for $C(T)/C(300\ \mathrm{K})$ and $I_{PL}(T)/I_{PL}(300\ \mathrm{K})$ from a model of the CW ESR experiments depending on $\tau_{m_s=0}(T)$ and $\tau_{m_s=\pm 1}(T)$.

decohere the spin at all but cryogenic temperatures [53]. We performed these measurements by polarizing the spin with a 532-nm CW laser pulse, coherently manipulating the spin with resonant microwaves, and reading out the spin state by monitoring the PL [1]. Both Rabi [Fig. 5(a)] and Ramsey pulse sequences were employed (see Supplemental Material [26] and Refs. [54,55]), demonstrating that the spin can be coherently controlled at temperatures exceeding 600 K and showing I_{PL} and ESR contrast trends consistent with the fluorescence quenching observed in our CW ESR measurements. Moreover, fits to

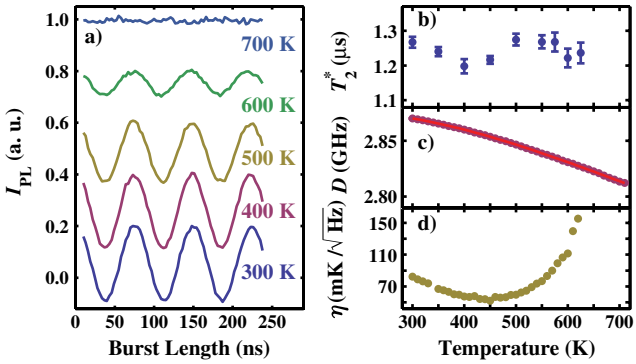

FIG. 5. (a) Rabi oscillations on the $m_s = 0$ to $m_s = -1$ transition at varying temperatures. The measurements are offset for clarity. (b) T_2^* versus temperature inferred from the decay envelope of fits to Ramsey oscillations. These measurements were performed at approximately 500 G to polarize the NV center's ^{14}N nuclear spin to simplify its hyperfine spectrum. All other measurements were performed at approximately 45 G. Error bars represent 68% intervals. (c) The crystal field splitting, $D(T)$, inferred from Lorentzian fits to the CW ESR data. The solid red line is the third-order polynomial fit to the data given in the main text. (d) Single-spin thermal sensitivity (η). η was calculated using Eq. (2) with all parameters from the same NV center.

the Ramsey oscillation decay envelope showed that T_2^* is temperature independent up to at least 625 K [Fig. 5(b)]. We also performed longitudinal relaxation measurements by optically polarizing the spin into $m_s = 0$ and measuring the relaxation into $m_s = \pm 1$ through the time-dependent I_{PL}. The measurements demonstrated that T_1 at 600 K (340 ± 50 μs) was still much longer than the period of the pulsed ESR measurements, confirming that spin relaxation does not explain the observed decrease in the ESR contrast and I_{PL}.

The persistence of the spin coherence and the strong temperature dependence of the crystal field splitting, D, suggest the possibility of using the spin resonances for thermometry. Based on our CW ESR measurements, we find that $D(T)$ [Fig. 5(c)] is accurately described by a third-order polynomial, $D(T) = a_0 + a_1 T + a_2 T^2 + a_3 T^3$, between 300 and 700 K, with $a_0 = (2.8697 \pm 0.0009)$ GHz, $a_1 = (9.7 \pm 0.6) \times 10^{-5}$ GHz/K, $a_2 = (-3.7 \pm 0.1) \times 10^{-7}$ GHz/K^2, and $a_3 = (1.7 \pm 0.1) \times 10^{-10}$ GHz/K^3. The derivative of this polynomial yields thermal shifts ranging from 80 kHz/K at 300 K to 170 kHz/K at 700 K. The possibility of spin-based thermometry is further motivated by the established methods for measuring small static shifts in the NV center spin resonance frequencies [8,9,56,57]. Perhaps the best known method for sensing such shifts is through a Ramsey measurement, in which a superposition of two spin states is created and evolves under the influence of static dephasing fields. After a time t, a microwave control pulse is applied to convert the accumulated phase into a population difference of the two spin states that can be read out optically.

We quantify the thermal sensitivity (η) based on our measurements of the defects's temperature-dependent optical and spin properties using an expression analogous to those derived for NV center dc magnetic-field-sensing with a Ramsey pulse sequence [58]:

$$\eta(T) = \frac{1}{2\pi \frac{dD(T)}{dT} A(T) \sqrt{T_2^*}}. \tag{2}$$

$A(T)$ accounts for the finite photon count rate and ESR contrast and is given by

$$A(T) = \left(1 + 2\frac{\alpha_0 + \alpha_1}{(\alpha_0 - \alpha_1)^2}\right)^{-1/2}, \tag{3}$$

where $\alpha_0 = \tau_{\mathrm{F}} I_{\mathrm{PL}}(T)$ and $\alpha_1 = \tau_{\mathrm{F}} I_{\mathrm{PL}}(T)[1 - C_{\mathrm{P}}(T)]$. Here τ_{F} is the fluorescence readout duration (350 ns) and $C_{\mathrm{P}}(T)$ is the contrast of a pulsed ESR measurement (0.24 for our Ramsey measurements). Based on the data presented in Figs. 4, 5(b), and 5(c), we find that $A(300\ \mathrm{K}) \sim 0.02$ and $\eta \sim 100\ \mathrm{mK}/\sqrt{\mathrm{Hz}}$ between room temperature and 600 K [Fig. 5(d)]. At higher temperatures, the sensitivity becomes limited by the quenching of the optical-spin readout. This sensitivity could be enhanced for NV centers in isotopically pure diamond, which can exhibit T_2^* times greater than 100 μs [59], corresponding to η better than $10\ \mathrm{mK}/\sqrt{\mathrm{Hz}}$.

These results demonstrate that NV centers offer operating temperatures and thermal sensitivities relevant to studies of thermal gradients in a variety of microscale and nanoscale systems. Recent demonstrations of the incorporation and quantum control of nanocrystal diamonds containing NV centers in living cells [60] suggest that NV centers could provide an alternative to quantum dot nanostructures for cellular thermometry [21]. In addition, as the ideal thermal and mechanical properties of diamond have motivated its use in scanning thermal microscopy tips [22], advances in the incorporation of NV centers in scanning probe tips [61,62] indicate the possibility of spin-based thermal microscopy for investigating materials such as nanostructured thermoelectrics [63,64]. Finally, given the large thermal shifts in D and the ability to optically polarize the spin at high temperatures, high-density ensembles of NV centers [65] could be used as an *in situ* thermometer for electron paramagnetic resonance experiments in analogy with chemical-shift thermometers used in nuclear magnetic resonance [66].

The results presented here provide fundamental insights on how thermally driven nonradiative processes can influence the fluorescence properties of defect-based spin qubits. We show that the NV center's fluorescence-based spin readout is ultimately limited above room temperature by nonradiative processes that diminish the spin-selectivity of its ^3E to $^1A_1$ orbital transition and upset the balance between the defect's radiative and nonradiative relaxation rates. Coupled with the persistence of its spin coherence, these measurements suggest that the NV center could find application as a nanoscale thermal sensor over a broad temperature range.

This work was funded by the AFOSR, ARO, and DARPA. We acknowledge computational resources at XSEDE. A portion of this work was done in the UCSB nanofabrication facility, part of the NSF-funded NNIN network. A. A. was supported by a grant from the Swiss NSF. D. M. T. and D. J. C. contributed equally to this work.

[1] F. Jelezko, T. Gaebel, I. Popa, A. Gruber, and J. Wrachtrup, *Observation of Coherent Oscillations in a Single Electron Spin*, Phys. Rev. Lett. **92**, 076401 (2004).

[2] G. Balasubramanian, P. Neumann, D. Twitchen, M. Markham, R. Kolesov, N. Mizuochi, J. Isoya, J. Achard, J. Beck, J. Tissler *et al.*, *Ultralong Spin Coherence Time in Isotopically Engineered Diamond*, Nature Mater. **8**, 383 (2009).

[3] A. Gruber, A. Dräbenstedt, C. Tietz, L. Fleury, J. Wrachtrup, and C. Borczyskowski, *Scanning Confocal Optical Microscopy and Magnetic Resonance on Single Defect Centers*, Science **276**, 2012 (1997).

[4] M. V. Dutt, L. Childress, L. Jiang, E. Togan, J. Maze, F. Jelezko, A. S. Zibrov, P. R. Hemmer, and M. D. Lukin, *Quantum Register Based on Individual Electronic and*

Nuclear Spin Qubits in Diamond, Science **316**, 1312 (2007).

[5] P. Neumann, J. Beck, M. Steiner, F. Rempp, H. Fedder, P. R. Hemmer, J. Wrachtrup, and F. Jelezko, *Single-Shot Readout of a Single Nuclear Spin*, Science **329**, 542 (2010).

[6] B. B. Buckley, G. D. Fuchs, L. C. Bassett, and D. D. Awschalom, *Spin-Light Coherence for Single-Spin Measurement and Control in Diamond*, Science **330**, 1212 (2010).

[7] L. Robledo, L. Childress, H. Bernien, B. Hensen, P. F. A. Alkemade, and R. Hanson, *High-Fidelity Projective Read-Out of a Solid-State Spin Quantum Register*, Nature (London) **477**, 574 (2011).

[8] J. R. Maze, P. L. Stanwix, J. S. Hodges, S. Hong, J. M. Taylor, P. Cappellaro, L. Jiang, M. V. G. Dutt, E. Togan, A. S. Zibrov *et al.*, *Nanoscale Magnetic Sensing with an Individual Electronic Spin in Diamond*, Nature (London) **455**, 644 (2008).

[9] G. Balasubramanian, I. Y. Chan, R. Kolesov, M. Al-Hmoud, J. Tisler, C. Shin, C. Kim, A. Wojcik, P. R. Hemmer, A. Krueger *et al.*, *Nanoscale Imaging Magnetometry with Diamond Spins under Ambient Conditions*, Nature (London) **455**, 648 (2008).

[10] F. Dolde, H. Fedder, M. W. Doherty, T. Nöbauer, F. Rempp, G. Balasubramanian, T. Wolf, F. Reinhard, L. C. L. Hollenberg, F. Jelezko *et al.*, *Electric-Field Sensing Using Single Diamond Spins*, Nature Phys. **7**, 459 (2011).

[11] J. H. N. Loubser and J. A. Van Wyk, *Optical Spin-Polarisation in a Triplet State in Irradiated and Annealed Type 1b Diamonds*, Diamond Research **1**, 11 (1977).

[12] D. A. Redman, S. Brown, R. H. Sands, and S. C. Rand, *Spin Dynamics and Electronic States of NV Centers in Diamond by EPR and Four-Wave-Mixing Spectroscopy*, Phys. Rev. Lett. **67**, 3420 (1991).

[13] J. R. Weber, W. F. Koehl, J. B. Varley, A. Janotti, B. B. Buckley, C. G. Van de Walle, and D. D. Awschalom, *Quantum Computing with Defects*, Proc. Natl. Acad. Sci. U.S.A. **107**, 8513 (2010).

[14] W. F. Koehl, B. B. Buckley, F. J. Heremans, G. Calusine, and D. D. Awschalom, *Room Temperature Coherent Control of Defect Spin Qubits in Silicon Carbide*, Nature (London) **479**, 84 (2011).

[15] N. B. Manson, J. P. Harrison, and M. J. Sellars, *Nitrogen-Vacancy Center in Diamond: Model of the Electronic Structure and Associated Dynamics*, Phys. Rev. B **74**, 104303 (2006).

[16] L. J. Rogers, S. Armstrong, M. J. Sellars, and N. B. Manson, *Infrared Emission of the NV Centre in Diamond: Zeeman and Uniaxial Stress Studies*, New J. Phys. **10**, 103024 (2008).

[17] V. M. Acosta, A. Jarmola, E. Bauch, and D. Budker, *Optical Properties of the Nitrogen-Vacancy Singlet Levels in Diamond*, Phys. Rev. B **82**, 201202 (2010).

[18] N. Manson, L. Rogers, M. Doherty, and L. Hollenberg, *Optically Induced Spin Polarisation of the NV-Centre in Diamond: Role of Electron-Vibration Interaction*, arXiv:1011.2840.

[19] L. Robledo, H. Bernien, T. van der Sar, and R. Hanson, *Spin Dynamics in the Optical Cycle of Single Nitrogen-Vacancy Centres in Diamond*, New J. Phys. **13**, 025013 (2011).

[20] Y. Ma, M. Rohlfing, and A. Gali, *Excited States of the Negatively Charged Nitrogen-Vacancy Color Center in Diamond*, Phys. Rev. B **81**, 041204 (2010).

[21] J. M. Yang, H. Yang, and L. Lin, *Quantum Dot Nano Thermometers Reveal Heterogeneous Local Thermogenesis in Living Cells*, ACS Nano **5**, 5067 (2011).

[22] A. Majumdar, J. Lai, M. Chandrachood, O. Nakabeppu, Y. Wu, and Z. Shi, *Thermal Imaging by Atomic Force Microscopy Using Thermocouple Cantilever Probes*, Rev. Sci. Instrum. **66**, 3584 (1995).

[23] J. P. Hadden, J. P. Harrison, A. C. Stanley-Clarke, L. Marseglia, Y. L. D. Ho, B. R. Patton, J. L. O'Brien, and J. G. Rarity, *Strongly Enhanced Photon Collection from Diamond Defect Centers under Microfabricated Integrated Solid Immersion Lenses*, Appl. Phys. Lett. **97**, 241901 (2010).

[24] L. Marseglia, J. P. Hadden, A. C. Stanley-Clarke, J. P. Harrison, B. Patton, Y. L. D. Ho, B. Naydenov, F. Jelezko, J. Meijer, P. R. Dolan *et al.*, *Nanofabricated Solid Immersion Lenses Registered to Single Emitters in Diamond*, Appl. Phys. Lett. **98**, 133107 (2011).

[25] G. D. Fuchs, V. V. Dobrovitski, D. M. Toyli, F. J. Heremans, and D. D. Awschalom, *Gigahertz Dynamics of a Strongly Driven Single Quantum Spin*, Science **326**, 1520 (2009).

[26] See Supplemental Material at http://link.aps.org/supplemental/10.1103/PhysRevX.2.031001 for additional details.

[27] R. J. Epstein, F. M. Mendoza, Y. K. Kato, and D. D. Awschalom, *Anisotropic Interactions of a Single Spin and Dark-Spin Spectroscopy in Diamond*, Nature Phys. **1**, 94 (2005).

[28] J. H. N. Loubser and J. A. Wyk, *Electron Spin Resonance in the Study of Diamond*, Rep. Prog. Phys. **41**, 1201 (1978).

[29] V. M. Acosta, E. Bauch, M. P. Ledbetter, A. Waxman, L. S. Bouchard, and D. Budker, *Temperature Dependence of the Nitrogen-Vacancy Magnetic Resonance in Diamond*, Phys. Rev. Lett. **104**, 070801 (2010).

[30] X.-D. Chen, C.-H. Dong, F.-W. Sun, C.-L. Zou, J.-M. Cui, Z.-F. Han, and G.-C. Guo, *Temperature Dependent Energy Level Shifts of Nitrogen-Vacancy Centers in Diamond*, Appl. Phys. Lett. **99**, 161903 (2011).

[31] B. Di Bartolo and X. Chen, *Advances in Nonradiative Processes in Solids* (Plenum Publishing Corporation, New York, 1991), Vol. 249.

[32] A. T. Collins, M. F. Thomaz, and M. I. B. Jorge, *Luminescence Decay Time of the 1.945 eV Centre in Type Ib Diamond*, J. Phys. C **16**, 2177 (1983).

[33] T. Plakhotnik and D. Gruber, *Luminescence of Nitrogen-Vacancy Centers in Nanodiamonds at Temperatures Between 300 and 700 K: Perspectives on Nanothermometry*, Phys. Chem. Chem. Phys. **12**, 9751 (2010).

[34] J. A. Vrugt, E. Laloy, C. J. F. ter Braak, and J. M. Hyman, Posterior Exploration Using Differential Evolution Adaptive Metropolis with Sampling from Past States (unpublished).

[35] E. Laloy and J. A. Vrugt, *High-Dimensional Posterior Exploration of Hydrologic Models Using Multiple-Try DREAM(ZS) and High Performance Computing*, Water Resour. Res. **48**, W01526 (2012).

[36] G. L. Bretthorst, W. C. Hutton, J. R. Garbow, and J. J. H. Ackerman, *Exponential Parameter Estimation (in NMR) Using Bayesian Probability Theory*, Concept. Magn. Reson. **27A**, 55 (2005).

[37] M. H. Chen and Q. M. Shao, *Monte Carlo Estimation of Bayesian Credible and HPD Intervals*, J. Comput. Graph. Stat. **8**, 69 (1999) http://www.jstor.org/stable/1390921.

[38] A. Gelman and D. B. Rubin, *Inference from Iterative Simulation Using Multiple Sequences*, Stat. Sci. **7**, 457 (1992).

[39] A. Gali, E. Janzén, P. Deák, G. Kresse, and E. Kaxiras, *Theory of Spin-Conserving Excitation of the N-V^- Center in Diamond*, Phys. Rev. Lett. **103**, 186404 (2009).

[40] J. Heyd, G. E. Scuseria, and M. Ernzerhof, *Hybrid Functionals Based on a Screened Coulomb Potential*, J. Chem. Phys. **118**, 8207 (2003).

[41] P. E. Blöchl, *Projector Augmented-Wave Method*, Phys. Rev. B **50**, 17953 (1994).

[42] G. Kresse and J. Furthmüller, *Efficiency of Ab Initio Total Energy Calculations for Metals and Semiconductors Using a Plane-Wave Basis Set*, Comput. Mater. Sci. **6**, 15 (1996).

[43] K.-M. C. Fu, C. Santori, P. E. Barclay, L. J. Rogers, N. B. Manson, and R. G. Beausoleil, *Observation of the Dynamic Jahn-Teller Effect in the Excited States of Nitrogen-Vacancy Centers in Diamond*, Phys. Rev. Lett. **103**, 256404 (2009).

[44] T. A. Abtew, Y. Y. Sun, B.-C. Shih, P. Dev, S. B. Zhang, and P. Zhang, *Dynamic Jahn-Teller Effect in the NV^- Center in Diamond*, Phys. Rev. Lett. **107**, 146403 (2011).

[45] T. Sato, K. Ohashi, T. Sudoh, K. Haruna, and H. Maeta, *Thermal Expansion of a High Purity Synthetic Diamond Single Crystal at Low Temperatures*, Phys. Rev. B **65**, 092102 (2002).

[46] A. Ranjbar, M. Babamoradi, M. Heidari Saani, M. A. Vesaghi, K. Esfarjani, and Y. Kawazoe, *Many-Electron States of Nitrogen-Vacancy Centers in Diamond and Spin Density Calculations*, Phys. Rev. B **84**, 165212 (2011).

[47] I. N. Levine, *Quantum Chemistry* (Prentice Hall, New Jersey, 1991).

[48] J. R. Maze, A. Gali, E. Togan, Y. Chu, A. Trifonov, E. Kaxiras, and M. D. Lukin, *Properties of Nitrogen Vacancy Centers in Diamond: The Group Theoretic Approach*, New J. Phys. **13**, 025025 (2011).

[49] M. W. Doherty, N. B. Manson, P. Delaney, and L. C. L. Hollenberg, *The Negatively Charged Nitrogen-Vacancy Centre in Diamond: The Electronic Solution*, New J. Phys. **13**, 025019 (2011).

[50] G. Davies and M. F. Hamer, *Optical Studies of the 1.945 eV Vibronic Band in Diamond*, Proc. R. Soc. A **348**, 285 (1976).

[51] A. Alkauskas *et al.* (unpublished).

[52] S. C. Rand, *Lectures on Light: Nonlinear and Quantum Optics Using the Density Matrix* (Oxford University Press, New York, 2010).

[53] L. Childress, M. V. Gurudev Dutt, J. M. Taylor, A. S. Zibrov, F. Jelezko, J. Wrachtrup, P. R. Hemmer, and M. D. Lukin, *Coherent Dynamics of Coupled Electron and Nuclear Spin Qubits in Diamond*, Science **314**, 281 (2006).

[54] V. Jacques, P. Neumann, J. Beck, M. Markham, D. Twitchen, J. Meijer, F. Kaiser, G. Balasubramanian, F. Jelezko, and J. Wrachtrup, *Dynamic Polarization of Single Nuclear Spins by Optical Pumping of Nitrogen-Vacancy Color Centers in Diamond at Room Temperature*, Phys. Rev. Lett. **102**, 057403 (2009).

[55] B. Smeltzer, L. Childress, and A. Gali, ^{13}C *Hyperfine Interactions in the Nitrogen-Vacancy Centre in Diamond*, New J. Phys. **13**, 025021 (2011).

[56] V. M. Acosta, E. Bauch, A. Jarmola, L. J. Zipp, M. P. Ledbetter, and D. Budker, *Broadband Magnetometry by Infrared-Absorption Detection of Nitrogen-Vacancy Ensembles in Diamond*, Appl. Phys. Lett. **97**, 174104 (2010).

[57] R. S. Schoenfeld and W. Harneit, *Real Time Magnetic Field Sensing and Imaging Using a Single Spin in Diamond*, Phys. Rev. Lett. **106**, 030802 (2011).

[58] J. M. Taylor, P. Cappellaro, L. Childress, L. Jiang, D. Budker, P. R. Hemmer, A. Yacoby, R. Walsworth, and M. D. Lukin, *High-Sensitivity Diamond Magnetometer with Nanoscale Resolution*, Nature Phys. **4**, 810 (2008).

[59] N. Zhao, J. Honert, B. Schmid, J. Isoya, M. Markham, D. Twitchen, F. Jelezko, R.-B. Liu, H. Fedder, and J. Wrachtrup, *Sensing Remote Nuclear Spins*, arXiv:1204.6513.

[60] L. P. McGuinness, Y. Yan, A. Stacey, D. A. Simpson, L. T. Hall, D. Maclaurin, S. Prawer, P. Mulvaney, J. Wrachtrup, F. Caruso, R. E. Scholten, and L. C. L. Hollenberg, *Quantum Measurement and Orientation Tracking of Fluorescent Nanodiamonds inside Living Cells*, Nature Nanotech. **6**, 358 (2011).

[61] P. Maletinsky, S. Hong, M. S. Grinolds, B. Hausmann, M. D. Lukin, R. L. Walsworth, M. Loncar, and A. Yacoby, *A Robust Scanning Diamond Sensor for Nanoscale Imaging with Single Nitrogen-Vacancy Centres*, Nature Nanotech. **7**, 320 (2012).

[62] L. Rondin, J. P. Tetienne, P. Spinicelli, C. Dal Savio, K. Karrai, G. Dantelle, A. Thiaville, S. Rohart, J. F. Roch, and V. Jacques, *Nanoscale Magnetic Field Mapping with a Single Spin Scanning Probe Magnetometer*, Appl. Phys. Lett. **100**, 153118 (2012).

[63] M. Soini, I. Zardo, E. Uccelli, S. Funk, G. Koblmüller, A. Fontcuberta i Morral, and G. Abstreiter, *Thermal Conductivity of GaAs Nanowires Studied by Micro-Raman Spectroscopy Combined with Laser Heating*, Appl. Phys. Lett. **97**, 263107 (2010).

[64] L. Shi, D. Li, C. Yu, W. Jang, D. Kim, Z. Yao, P. Kim, and A. Majumdar, *Measuring Thermal and Thermoelectric Properties of One-Dimensional Nanostructures Using a Microfabricated Device*, J. Heat Transfer **125**, 881 (2003).

[65] V. M. Acosta, E. Bauch, M. P. Ledbetter, C. Santori, K.-M. C. Fu, P. E. Barclay, R. G. Beausoleil, H. Linget, J. F. Roch, F. Treussart, S. Chemerisov, W. Gawlik, and D. Budker, *Diamonds with a High Density of Nitrogen-Vacancy Centers for Magnetometry Applications*, Phys. Rev. B **80**, 115202 (2009).

[66] A. Bielecki and D. P. Burum, *Temperature Dependence of* ^{207}Pb *MAS Spectra of Solid Lead Nitrate. An Accurate, Sensitive Thermometer for Variable-Temperature MAS*, J. Magn. Reson., Ser. A **116**, 215 (1995).